PHYSICAL REVIEW C **88**, 021901(R) (2013)

Universal hadronization condition in heavy ion collisions at $\sqrt{s_{NN}} = 62$ GeV and at $\sqrt{s_{NN}} = 2.76$ TeV

Michal Petráň and Johann Rafelski
Department of Physics, The University of Arizona, Tucson, Arizona 85721, USA
(Received 4 March 2013; revised manuscript received 25 April 2013; published 16 August 2013)

We obtain a detailed description of all available hadron multiplicity yields in central Pb-Pb collisions at the CERN Large Hadron Collider (LHC) measured in the rapidity interval $|y| < 0.5$. We find that the hadronization of the fireball at the LHC occurs at nearly identical intensive physical bulk conditions for all centralities similar to those already seen at the Brookhaven National Laboratory Relativistic Heavy Ion Collider.

DOI: 10.1103/PhysRevC.88.021901 PACS number(s): 25.75.Nq, 24.10.Pa, 12.38.Mh

Introduction and motivation. We extend the successful description of central rapidity particle yields in a single freeze-out model [1,2] to characterize the physical properties of the hadronizing fireball. We consider, as an example, a supercooled quark-gluon plasma (QGP) disintegrating into hadrons, which can scatter but can preserve the stable particle abundance. Therefore, hadron particle multiplicities directly characterize the properties of the fireball. Final state hadrons are, thus, produced according to the accessible phase space with otherwise equal reaction strength. Accordingly, the particle yields are described by the chemical non-equilibrium statistical hadronization model (SHM) [3].

In this SHM implementation within the SHAREV2.2 program, the yields of particles are given the chemical freeze-out temperature T and overall normalization dV/dy (matching the presentation of the experimental data available as dN/dy). We include phase-space occupancies γ_q, γ_s for light ($q = u, d$) and strange s quark flavors, respectively, and we account for the small asymmetry between particles and antiparticles by fugacity factors λ_q, λ_s and the light quark asymmetry λ_{I3}. These parameters enter the distribution function as $f_i(\varepsilon, T, \gamma_i, \lambda_i) = 1/(\gamma_i^{-1}\lambda_i^{\pm 1}e^{\varepsilon/T} + S)$ for flavor i, where $S = -1, 0, +1$ for bosons, Boltzmann distribution, and fermions, respectively. We refer the reader to Sec. 2 of Ref. [4] for further discussion of the above parameters.

Our discussion addresses, evaluates, and compares the CERN Large Hadron Collider (LHC) Pb-Pb experimental results available at $\sqrt{s_{NN}} = 2760$ GeV and the Brookhaven National Laboratory Relativistic Heavy Ion Collider (RHIC) Au-Au results available at $\sqrt{s_{NN}} = 62.4$ GeV. We show that the chemical non-equilibrium SHM works at the LHC in the 0–20% centrality. This is so, since in the chemical non-equilibrium SHM approach, we allow the quark pair yield parameter $\gamma_q > 1$ for light quarks; this is the key difference from the simpler equilibrium SHM. The rationale for $\gamma_q \neq 1$ originates in the high entropy density of QGP at hadronization compared to the hadron phase space in which the color degree of freedom is frozen. In case the fireball disintegrates faster than the time necessary to equilibrate the yield of light quarks bound in hadrons, the value $\gamma_q > 1$ must arise.

In case the fireball disintegrates faster than the time necessary to equilibrate the yield of light quarks bound in hadrons, either the value $\gamma_q > 1$ arises, or one must consider a dynamical volume growth as a path for absorbing the excess entropy of the QGP source. However, this second option requires a much longer life span of the particle source than supported by the two pion correlation data [5,6] and, thus, is experimentally excluded: The observed LHC total life span ($\tau_f \simeq 10$ fm/c [6]) favors very fast, or sudden, hadronization [7,8]. In this situation, the chemical non-equilibrium approach must also be applied to the light quark abundance, which introduces the light quark phase-space occupancy γ_q. This proposal, made for the high-energy CERN Super Proton Synchrotron (SPS) data [9,10], also helped to improve the understanding of RHIC200 hadron rapidity yield results [11] and allowed a consistent interpretation of such data across the full energy range at the SPS and RHIC200 [12].

The equilibrium SHM fits, which arbitrarily set $\gamma_q = 1$ [13,14], describe hadron yields at the LHC with relatively large total χ^2. This chemical equilibrium SHM disagrees at the LHC across many particle yields, but the greatest issue is the "proton anomaly," which makes it impossible to fit the $p/\pi = 0.046 \pm 0.003$ ratio [14] along with the multistrange baryons Ξ and Ω.

We will show that intensive QGP bulk properties are nearly exactly equal to those found at the RHIC for all four collision centralities we analyze. We will discuss in depth the main extensive bulk property difference we find, which is the entropy dS/dy growth with energy and centrality.

Fit to most central collisions. Within the chemical non-equilibrium SHM, we have, by allowing for baryon-antibaryon asymmetry, seven independent statistical model parameters reduced by two constraints: (a) The isospin fugacity factor λ_{I3} is constrained by imposing the charge per baryon ratio $(\langle Q\rangle - \langle\overline{Q}\rangle)/(\langle B\rangle - \langle\overline{B}\rangle) \simeq 0.38$, present in the initial nuclear matter state at the initial instant of the collision; (b) for each value of λ_q, strangeness fugacity λ_s is evaluated by imposing the strangeness conservation requirement $\langle s\rangle - \langle\bar{s}\rangle \simeq 0$. By considering the particle-antiparticle symmetry at the LHC, the four key parameters are the hadronization volume dV/dy, the temperature T, and the two phase-space occupancies γ_q and γ_s. The seventh parameter is light quark fugacity λ_q.

We use, as input to our fit, the hadron yield data in the 0–20% centrality bin as presented in Ref. [15] where a fit to this data set for the case of chemical equilibrium ($\gamma_s = \gamma_q = 1$) is shown. For comparison and demonstration

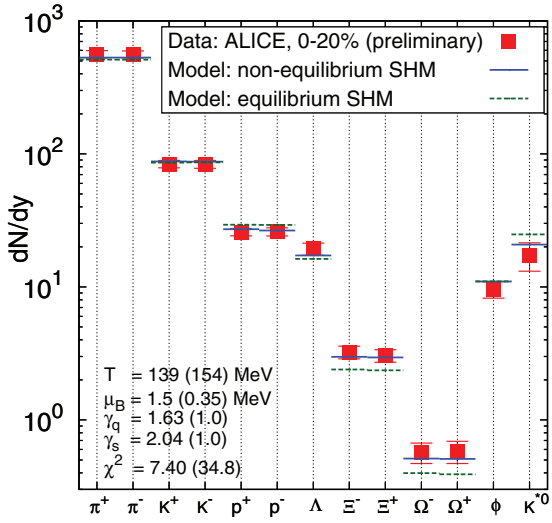

FIG. 1. (Color online) The non-equilibrium SHM fit is indicated by (blue) solid horizontal lines overlaying for all the LHC-ALICE (preliminary) data available in a 0–20% centrality bin (red squares). The chemical equilibrium fit is indicated by (green) dashed lines with model parameters presented in parentheses.

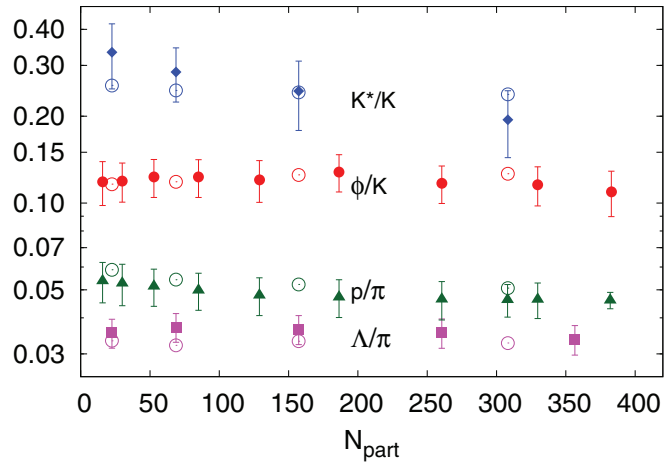

FIG. 2. (Color online) Experimental data (full symbols) and model predicted (open circles) for particle ratios as a function of centrality. See text for discussion of data and results.

of method compatibility, the chemical equilibrium model fit (dashed lines in Fig. 1) is shown with a large $\chi^2 = 34.8$. In both approaches, we fit the same data, the decrease in χ^2 by a factor of nearly 5 is due to chemical non-equilibrium, i.e., $\gamma_q \neq 1$, $\gamma_s \neq 1$. We determine the best light quark fugacity factor $\lambda_q = 1.003\,59$, which corresponds to the baryochemical potential $\mu_B \simeq 1.5$ MeV, and we apply strangeness and charge per baryon conservation by fitting them as two additional data points. The result of our 0–20% centrality bin fit is shown in Fig. 1 and in the upper section of the third column of Table I. We compare our present results to our recent analysis [16] of Au-Au collisions at $\sqrt{s_{NN}} = 62.4$ GeV at RHIC62, shown in the second column of Table I.

More peripheral centralities. We extend our study to more peripheral collisions at the LHC by using a much smaller data set, complemented by two assumptions as follows:

(i) We consider the three ratios K^{*0}/K^-, $\Lambda/\pi \equiv 2\Lambda/(\pi^- + \pi^+)$, and ϕ/K^- as presented in Ref. [17] and which we show in Fig. 2 with full symbols. We fit these ratios in three centrality bins, 20–40%, 40–60%, and 60–80% in which K^*/K and Λ/π have experimental data points. We take the average of two neighboring ϕ/K data points to use this ratio as input to our fit in the intermediate centrality. This is consistent with the claim that ϕ/K is constant over all centralities and has been claimed independent of centrality in Ref. [17].

(ii) To obtain overall normalization, we complement the ratios with charged particle rapidity density $dN_{\rm ch}/dy$. Based on our fit of 0–20% centrality data, we see that

TABLE I. The top section shows chemical non-equilibrium SHM fit parameters dV/dy, T, γ_q, γ_s, and $\chi^2_{\rm total}$ with number of data less number of parameters (ndf) obtained in each centrality bin. Errors are a fit-stability estimate obtained with a $K^\pm$ yield shifted within the experimental error; the underlying statistical fit error is negligible. The bottom section presents fireball bulk properties in each bin: energy density ε, pressure P, entropy density σ, strangeness per entropy content s/S, and entropy at LHC2760 compared to RHIC62 $S_{\rm LHC}/S_{\rm RHIC}$. The centrality that defines number of participants $N_{\rm part}$ values is adopted from Ref. [20].

	RHIC62	LHC2760			
Centrality	0–5%	0–20%	20–40%	40–60%	60–80%
$\langle N_{\rm part}\rangle$	346	308	157	68.8	22.6
dV/dy (fm^3)	853	2455 ± 146	1169 ± 9	406 ± 3	102 ± 7
T (MeV)	139.5	138.6 ± 1.1	137.6 ± 0.03	140.5 ± 0.04	143.2 ± 0.08
γ_q	1.58	1.627 ± 0.007	1.633 ± 0.0002	1.616 ± 0.003	1.60 ± 0.02
γ_s	2.24	2.04 ± 0.04	2.01 ± 0.12	1.83 ± 0.08	1.70 ± 0.09
$\chi^2_{\rm total}$/ndf	0.38/5	7.40/8	2.93/5	3.58/5	5.43/5
ε (GeV/fm^3)	0.493	0.466 ± 0.018	0.441 ± 0.012	0.488 ± 0.010	0.536 ± 0.025
P (MeV/fm^3)	82.0	79.1 ± 2.8	75.5 ± 1.5	82.2 ± 1.3	90.2 ± 4.0
σ (fm^{-3})	3.40	3.23 ± 0.11	3.07 ± 0.07	3.36 ± 0.06	3.65 ± 0.13
s/S	0.0322	0.0296 ± 0.0002	0.0289 ± 0.0014	0.0277 ± 0.0009	0.0267 ± 0.0011
$S_{\rm LHC}/S_{\rm RHIC}$		3.05	2.66	2.18	1.52

the ratio of charged particle rapidity to pseudorapidity density is $(dN_{\rm ch}/dy)/(dN_{\rm ch}/d\eta) = 1.115$. We multiply data from Ref. [18] by this factor and use the resulting $dN_{\rm ch}/dy$ as an additional data point that determines the value of fireball volume dV/dy. The input multiplicity data is presented in Fig. 3.

(iii) We include the yields of $\pi^{\pm}$, $K^{\pm}$, and $p^{\pm}$ as presented in Ref. [19] and shown in Fig. 3. Similar to the ϕ/K ratio, we use the averages of yields in two neighboring centrality bins as input.

We fit the three centrality bins of the LHC2760 data by using the eight data points and the two conservation laws, which fix λ_s and λ_{I3}. Therefore, we have five degrees of freedom as seen in Table I in the fourth through sixth columns. All studied centralities show reasonable $\chi^2/{\rm ndf} \leqslant 1.1$. We find remarkably similar statistical parameters for all four LHC centrality bins.

We compare the outcome of the fit by showing the three input ratios K^{*0}/K^-, Λ/π, and ϕ/K^- and p/π in Fig. 2. All data are well fitted, including both yields of p and π from Ref. [19], which implies good description of their ratio p/π evaluated from the individual yields.

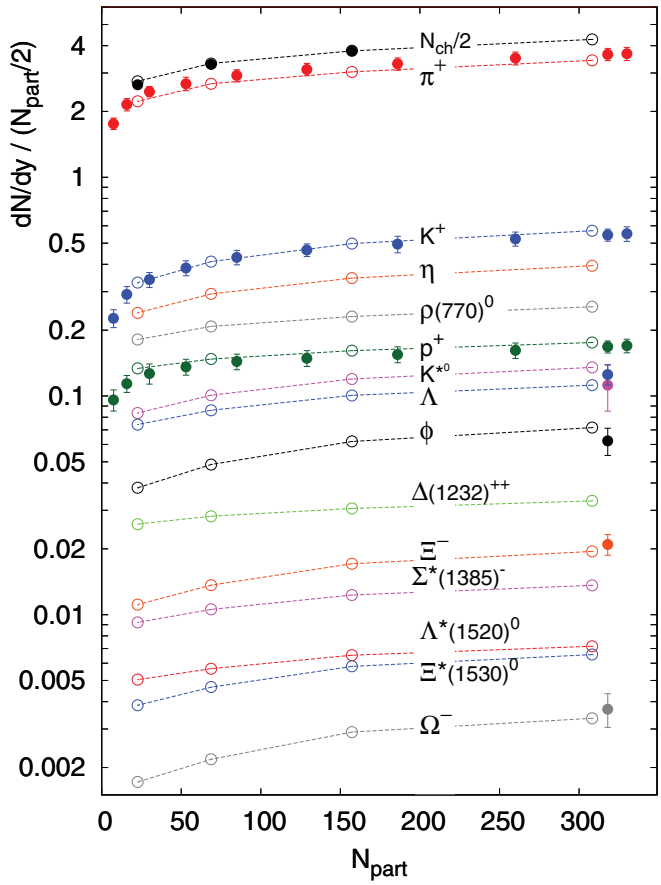

FIG. 3. (Color online) Predicted particle yields per participant pair as a function of centrality. Open symbols represent our model predictions; lines guide the eye. We show experimental data for the 0–20% bin as full symbols with an offset.

The predicted particle yields normalized by $N_{\rm part}/2$ are shown in Fig. 3 where, in consideration of particle-antiparticle symmetry, only one of the isospin multiplets is shown. The π, K, and p yields are fitted values, whereas, the other particle yields are predictions. In Fig. 3 on the right boundary, we indicate the experimental input for the 0–20% bin with an offset to assure visibility of the small differences between fit and experimental data. We show the input multiplicity $(dN_{\rm ch}/dy)/(N_{\rm part}/2)$ and fit result in Fig. 3. Both are exactly overlapping for the three peripheral bins since this is the most precise input data.

Hadronization conditions. Despite a change by a factor of 45 in the reaction energy by comparing the RHIC and the LHC and the wide range of centrality, the only quantity among the statistical parameters shown in Table I that significantly changes is dV/dy. This suggests that we should look closer at the intensive bulk physical properties of the fireball: The emitted hadrons not only carry the above-discussed charge, baryon number, or strangeness away from the fireball, but also, e.g., carry the thermal energy dE/dy obtained by summing the energy content of all produced particles, observed and predicted.

The bulk thermal energy density at hadronization ε defined by $\varepsilon \equiv (dE/dy)/(dV/dy)$ is of direct interest. Similarly, we evaluate the entropy dS/dy, pressure P, and total yield of strangeness $ds/dy \equiv d(q_s + \bar{q}_s)/2\,dy$. These properties of the fireball at hadronization are shown in the bottom section of Table I where, in the first column, for simplicity, we omit the symbol d/dy.

As one can see by comparing the second and third columns of Table I, the intensive properties of the RHIC62 fireball at hadronization, i.e., ε, P, σ, and s/S, are practically identical to the here evaluated case of LHC2760, and this continues across all considered centralities as seen in the fourth through sixth columns of Table I. We show a comparison of ε, P as a function of centrality between the LHC (solid symbols) and the RHIC (open symbols) in the bottom part of Fig. 4. The difference between the LHC and the RHIC can easily be attributed to the fit uncertainties since the intensive quantities are proportional to a high power of statistical parameters.

Hadronization volume dV/dy does not characterize the early stage of a collision; this information is available in the entropy content at hadronization $dS/dy \propto dV/dy$, which presents a more accurate view of the prehadronization processes that created the fireball. For an ideally flowing and expanding QGP, most of the observed entropy yield dS/dy of a fireball is created early in the collision. In the top panel of Fig. 4, we see that, at the LHC, $dS/dy \propto N_{\rm part}^{\sim 1.173}$, the rise is faster than linear. For comparison, note that, at the RHIC, the entropy yield rises almost linearly with $N_{\rm part}$. The last row of Table I shows the enhancement of entropy at the LHC compared to the RHIC $S_{\rm LHC}/S_{\rm RHIC}$. The enhancement decreases as a function of centrality from ~ 3 to ~ 1.5, which implies an additional entropy production mechanism proportional to centrality at the LHC.

Strangeness per entropy $s/S \equiv (ds/dy)/(dS/dy)$ is of particular interest in the source fireball since both entropy and

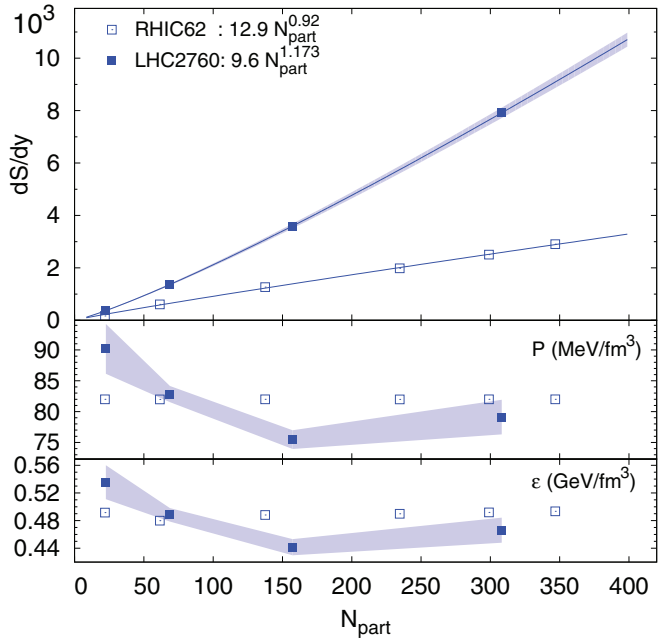

FIG. 4. (Color online) The top panel shows the entropy content of the fireball at the LHC (full symbols) and the RHIC (open symbols) as a function of centrality. The bottom part shows pressure P and energy density ε at hadronization with the same symbols for the LHC and the RHIC as in the top panel, for values, see Table I.

strangeness yields are nearly preserved in the hadronization process, but the production of strangeness occurs after most of the entropy is created. Up to a well-studied proportionality factor, s/S is the ratio of strange quark abundance to total quark and gluon abundance, which makes up the entropy in the bulk. Therefore, s/S measures the degree of chemical equilibration in the QGP. We observe a constant value of $s/S \simeq 0.03$ (see Table I), which is in agreement with theoretical expectations for the strange quark mass $m_s \simeq 100$ MeV [21].

Comments and conclusions. The LHC2760 experimental environment has opened a new opportunity to investigate the hadron production mechanisms in detail. Precise particle tracking near the interaction vertex in the ALICE removes the need for off-line corrections of weak interaction decays, and at the same time, vertex tracking enhances the efficiency of track identification by considerably increasing the precision of the particle yield measurement [13,15]. All LHC experimental results we considered were obtained in this way by the ALICE experiment for Pb-Pb collisions at $\sqrt{s_{NN}} = 2.76$ TeV, limited to the central unit of rapidity interval $-0.5 < y < 0.5$.

In this new experimental environment, we show the necessity to introduce the final-state hadron chemical non-equilibrium, which well describes all experimental results obtained in the Pb-Pb collisions at $\sqrt{s_{NN}} = 2.76$ TeV from the LHC. As Fig. 1 shows, $\gamma_q \simeq 1.6$ (non-equilibrium of light quarks) allows for describing the ratio $p/\pi = 0.046 \pm 0.003$ [13,14] together with yields of multistrange baryons Ξ and Ω.

Another approach to describe the data that include the "anomalous" proton yield at the LHC involves chemical equilibrium hadronization at relatively high T followed by hadron interactions [22,23]. We note the chemical equilibrium SHM yields at hadronization in Fig. 1, which overpredicts proton yield and, at the same time, underpredicts both Ξ and Ω. Any alternate data explanation must come to terms with this situation, thus, it must deplete protons and enhance both Ξ and Ω, and at the same time, the ratio p/π must remain practically constant. This is difficult, as we now discuss, by looking closer at the results of Refs. [22,23]:

(i) In Fig. 1 of Ref. [22], we see that if and when equilibrium style hadronization occurs and leads to high T, the necessary posthadronization reactions deplete protons and Ξ and enhance Ω. This means that the already too small yield of Ξ is further depleted and disagrees gravely with experiment.

(ii) The measured p/π ratio in the 0–5% centrality bin can be made consistent with posthadronization proton-antiproton annihilation [23]. This fine-tunes the model parameters and, as a result, for the 20–30% centrality bin, Ref. [23] reports increased $p/\pi = 0.058$.

(iii) For peripheral collisions, the model predicts yet less annihilation and, thus, a p/π ratio that approaches the equilibrium SHM value, which is twice as large as experiment. Although the experiment for p/π seen in Fig. 2 is a constant for all centralities, Ref. [23], thus, predicts a rapid variation by about factor of 2.

These arguments lead to the conclusion that posthadronization interactions are inconsistent with the experimental data of baryon yields at the LHC. On the other hand, our chemical non-equilibrium SHM at the LHC produces a high confidence level fit $\chi^2/\text{ndf} = 7.4/8 < 1$. Prior SPS and RHIC data analyses [11,12,16] have already strongly favored a chemical non-equilibrium variant of SHM. The implied sudden hadronization picture is perfectly consistent with the anisotropic flow of quarks that lead to the final hadron momentum distribution azimuthal asymmetry (see, e.g., Ref. [24]).

Moreover, we find that the LHC and RHIC results are quite consistent in our approach, and we obtain the same hadronization condition (ε, P, σ) at the LHC as previously reported at the RHIC, which, in turn, agrees with high-energy SPS [12]. The energy density of hadronizing matter is 0.50 ± 0.05 GeV/fm^3, which is about 3.3 times the energy density of nuclear matter, and the pressure is $P = 82 \pm 8$ MeV/fm^3 $= (158 \pm 4$ MeV$)^4$ as seen in the bottom part of Fig. 4, and which has been proposed in Ref. [25]. The bottom part of Table I also shows that the entropy density is constant: $\sigma = 3.35 \pm 0.30$ fm^{-3} for both experiments and all centralities.

These typical QGP properties, which include $s/S \to 0.03$, mean that, at the LHC, the source of hadrons is a chemically equilibrated strangeness saturated QGP fireball. Furthermore, the universal hadronization condition assures that hadron production cannot be viewed anymore as being due to successive particle emission or to proceed via the equilibrated hadron gas phase.

This work was supported by a grant from the US Department of Energy, Grant No. DE-FG02-04ER41318.

[1] M. Rybczyński, W. Florkowski, and W. Broniowski, Phys. Rev. C **85**, 054907 (2012).
[2] W. Broniowski and W. Florkowski, Phys. Rev. Lett. **87**, 272302 (2001).
[3] G. Torrieri, S. Steinke, W. Broniowski, W. Florkowski, J. Letessier, and J. Rafelski, Comput. Phys. Commun. **167**, 229 (2005); G. Torrieri, S. Jeon, J. Letessier, and J. Rafelski, *ibid.* **175**, 635 (2006).
[4] J. Rafelski, Eur. Phys. J. Spec. Top. **155**, 139 (2008).
[5] L. P. Csernai, M. I. Gorenstein, L. L. Jenkovszky, I. Lovas, and V. K. Magas, Phys. Lett. B **551**, 121 (2003).
[6] K. Aamodt (ALICE Collaboration) *et al.*, Phys. Lett. B **696**, 328 (2011).
[7] L. P. Csernai and I. N. Mishustin, Phys. Rev. Lett. **74**, 5005 (1995).
[8] J. Rafelski and J. Letessier, Phys. Rev. Lett. **85**, 4695 (2000).
[9] J. Letessier and J. Rafelski, Phys. Rev. C **59**, 947 (1999).
[10] J. Letessier and J. Rafelski, Int. J. Mod. Phys. E **09**, 107 (2000).
[11] J. Rafelski, J. Letessier, and G. Torrieri, Phys. Rev. C **72**, 024905 (2005).
[12] J. Letessier and J. Rafelski, Eur. Phys. J. A **35**, 221 (2008).
[13] B. Abelev (ALICE Collaboration), Proceedings from Physics of the LHC 2012 Conference (unpublished).
[14] B. Abelev (ALICE Collaboration) *et al.*, Phys. Rev. Lett. **109**, 252301 (2012).
[15] M. Ivanov (ALICE Collaboration), Nucl. Phys. A **904–905**, 162c (2013).
[16] M. Petran, J. Letessier, V. Petracek, and J. Rafelski, Acta Phys. Pol. B Proc. Suppl. **5**, 255 (2012).
[17] S. Singha (ALICE Collaboration), Nucl. Phys. A **904–905**, 539c (2013).
[18] K. Aamodt (ALICE Collaboration) *et al.*, Phys. Rev. Lett. **106**, 032301 (2011).
[19] B. Abelev (ALICE Collaboration) *et al.*, arXiv:1303.0737.
[20] B. Abelev (ALICE Collaboration) *et al.*, arXiv:1301.4361.
[21] I. Kuznetsova and J. Rafelski, Eur. Phys. J. C **51**, 113 (2007).
[22] J. Steinheimer, J. Aichelin, and M. Bleicher, Phys. Rev. Lett. **110**, 042501 (2013).
[23] I. A. Karpenko, Y. M. Sinyukov, and K. Werner, Phys. Rev. C **87**, 024914 (2013).
[24] U. W. Heinz and R. Snellings, Annu. Rev. Nucl. Part. Sci. **63**, 123 (2013).
[25] J. Rafelski and J. Letessier, J. Phys. G **36**, 064017 (2009).